Threshold estimation of an organic laser diode using a rate-equation model validated experimentally with a microcavity OLED submitted to nanosecond electrical pulses

Amani Ouirimi, Alex Chamberlain Chime, Nixson Loganathan, Mahmoud Chakaroun, Alexis P.A. Fischer, Daan Lenstra

Threshold estimation of an Organic Laser Diode using a rate-equation model validated experimentally with a microcavity OLED submitted to nanosecond electrical pulses

Amani Ouirimi[1,2], Alex Chamberlain Chime[1,2,3], Nixson Loganathan[1,2], Mahmoud Chakaroun[1,2], Alexis P. A. Fischer[1,2], Daan Lenstra[4]

1: Université Sorbonne Paris Nord, Laboratoire de Physique des Lasers, UMR CNRS 7538, 99 avenue JB Clement, 93430 Villetaneuse-F

2: Université Sorbonne Paris Nord , Centrale de Proximité en Nanotechnologies de Paris Nord, 99 avenue JB Clement, 93430 Villetaneuse-F

3: Université de Dschang, IUT-FV de Bandjoun, Cameroun

4: Institute of Photonics Integration, Eindhoven University of Technology, P.O. Box 513, 5600MB Eindhoven, The Netherlands

Abstract: We propose a new model for the organic laser diode based on rate equations for polarons, singlet and triplet excitons for both host and guest molecules, and photon densities. The proposed model is validated experimentally by comparing calculated and measured optical responses in the context of pulsed nanosecond electrical excitation of high-speed µ-OLEDs in the limit of weak micro-cavity effects. We predict the laser threshold current density as a function of the micro-cavity quality factor, for two material gain and residual absorption values. We elucidate the crucial role played by the latter in setting the laser threshold and comment on the recently observed threshold value of ~500 A/cm^2 by the group of Adachi [1]. Simulations predict that laser action under short electrical nanosecond pulse single-shot excitation is accompanied by damped relaxation oscillations in the GHz regime. The measured ultra-short experimental optical responses at 45V are best reproduced numerically when the Langevin recombination rate is larger than usually observed in the literature as a consequence of the field dependence of the Poole-Frenkel law for the mobility.

Keywords: Optoelectronics, OLED, laser, organic laser diode, laser dynamics

I. Introduction

Recently, Adachi and co-workers have reported indications of stimulated emission in an organic hetero-structure under electrical excitation [1]. Many aspects of this pioneering work need to be explored further and confirmed; for example, the reported current threshold is as low as 0.5 kA/cm^2, the laser linewidth reduction is incomplete, and the cavity structure remains to be described in more detail. However, this new organic laser diode (OLD) opens a new era in the field of lasing. Firstly because solid-state organic materials, contrary to their III-V counterparts, cover continuously the whole visible spectrum as well as part of the IR and UV spectrum. Secondly, they can be deposited more easily on almost any substrate with less energy consumption for the manufacturing process than conventional epitaxially-grown III-V materials. Thirdly, this new device combines properties from dye-lasers and solid-state diode lasers and as such will open new perspectives and potential applications.

With regard to perspectives, organic materials exhibit dependence of the refractive index on the carrier density different from conventional III-V semiconductors, which is very likely due to the specific mobility of disordered organic semiconductors [2, 3]. Therefore, new and interesting dynamical behaviour will occur, especially when the laser is submitted to different types of external perturbations, such as optical injection and feedback [4]. Regarding the potential applications and new possibilities, they will be facilitated by the ease of deposition of organic hetero-structures on a large variety of substrates including silicon, silica, glass, as well as flexible substrates, by the availability of an almost unlimited library of electroluminescent organic materials [5].

To further widen this new field, an overall understanding and description of the OLD mechanism provided by a unifying model is necessary. Such a model should be simple enough to facilitate its dissemination in different scientific communities, yet accurate enough to be useful in the establishment of design and fabrication rules. It should include electrical excitation instead of optical excitation and allow threshold estimation.

A first dynamical model has been introduced by Gärtner et al. [6]. Among the few dynamical models, Kasemann et al. proposed a simple rate equation model for the different exciton mechanisms in an OLED under pulsed electrical excitation, which provides a useful starting point [7]. However, it lacks inclusion of the micro-cavity and stimulated emission. The model introduced by Chua et al, does include the micro-cavity effect but pertains to optical pumping [8] and to time scales much longer than the nanosecond range considered in the current work.

In a very recent paper by Ahmad et al. [9] a theoretical and experimental investigation is reported of the polaron and exciton dynamics in Super Yellow OLEDs at high current-density nanosecond pulses. Apart from analysing the transient electrical current response of OLEDs to high voltage excitations, they focus on the dynamics of the spatial distributions of polaron charges, electric field and excitons and stimulated emission is not considered.

The goal of this paper is to set a first step toward a unified and simple model of the OLD that will be helpful in providing guidelines for the design and fabrication. As a second step, the validity and accuracy of the model are tested by confronting its predictability with measurements of an OLED with weak micro-cavity effect, under single-shot pulsed and intense electrical excitation in the nano-second range.

Contrary to Ahmad's work, we will deliberately assume for simplicity of the model that the densities of all constituents, i.e. polarons, excitons and photons, are uniformly distributed throughout the recombination zone with strict charge neutrality. Thus, our theory should be considered a first-order approximation.

As will be shown in Sec. II.J, in case of electrical excitation the build-up of triplet excitons becomes dominant after a few nanoseconds, at the expense of singlet excitons, where the latter are essential for the optical gain. Therefore, lasing should be expected to occur within a few nanoseconds whereas this applies to a much lesser extent to optical pumping. Therefore this study will focus on short time range typically 1 to 20ns.

A novelty of the current work is to introduce for the first time a laser model borrowed from the laser-dynamics field and to apply it to organic semiconductors in order to link the stimulated emission to the electrical excitation. The proposed OLD model can be applied to calculate the optical responses to electrical pulse excitations of guest-host system-based organic optoelectronic light sources and confront the predictions with the corresponding measured signal in the nano-second time scale. Our model also provides a framework to analyse indications of lasing of the OLD and the required threshold current density [1].

The paper is structured as follows: In section II the OLD model is presented based on rate equations for the various relevant variables. The interplay between host and dopant guest molecules is explicitly addressed. In the various subsections II.A to II.F the different physical entities, i.e. polarons, singlet and triplet excitons in the host and dopant separately, and the photons are discussed. The optical gain is discussed in Sec. II.G and an important factor, which plays a crucial role in the re-absorption of the (red) light emitted by the dopant singlet excitons is discussed in Sec. II.H. In Sec. II.I a few comments are given on the relation between the quality factor (Q) of the cavity and the corresponding photon lifetime. In Sec. II.J numerical results are presented and compared for cases without cavity, i.e. for low-Q, and with a high-Q cavity. A numerical demonstration of light emission from an electrically driven OLD above laser threshold is given for the first time.

Measurements of the electrical and optical responses of high-speed μ-OLED with weak micro-cavity under high current density single-shot nano-pulse excitation are presented in section III and compared with the predictions of the model. This enables validation of our model. In section IV, laser threshold densities are calculated and predicted for two different values of the gain parameter and compared with that reported by Adachi's group [1]. The conclusion is given in section V.

II. The model

In the model we assume that the hole-type and electron-type polarons participate in charge transfer across the different organic layers and recombine in the emitting layer to form singlet and triplet excitons. The singlets can decay radiatively by photon emission, whereas radiative decay is Pauli-forbidden for the triplets.

We consider the situation where the emitting layer is composed of host molecules (the matrix), doped with a few percent of guest molecules (the dopant), where the excitonic states are quickly transferred from the host molecules to the singlet and triplet excitons of the dopant molecules by Förster transfer and in a less extent by Dexter transfer [10]. With a guest-host system like Alq3:DCM, the host singlets have their optical transition in the green part of the spectrum (Alq3: ~520nm), whereas the dopant singlets provide both spontaneous and stimulated emission in the red spectrum (DCM: ~620nm). The idea is that the dopant-molecule ground states are easy to empty such that re-absorption of emitted light no longer hampers the optical gain, as it would do in case of host neat film.

The proposed OLD dynamical model is partially inspired on [6, 7, 8, 11, 12, 13]. The equations read

$$(1)\quad \frac{d}{dt}N_P = \frac{J(t)}{ed} - \gamma N_P^2$$

$$(2)\quad \begin{aligned}\frac{dN_S}{dt} &= \frac{1}{4}\gamma N_P^2 + \frac{1}{4}\kappa_{TT}N_T^2 \\ &\quad - \left(\kappa_{FRET}P_{0D} + \kappa_S + \kappa_{ISC}\right)N_S \\ &\quad - \left(\frac{7}{4}\kappa_{SS}N_S + \kappa_{SP}N_P + \kappa_{ST}N_T\right)N_S\end{aligned}$$

$$(3)\quad \begin{aligned}\frac{dN_T}{dt} &= \frac{3}{4}\gamma N_P^2 + \kappa_{ISC}N_S + \frac{3}{4}\kappa_{SS}N_S^2 \\ &\quad - \left(\kappa_{DEXT}P_{0D} + \kappa_T + \kappa_{TP}N_P\right)N_T \\ &\quad - \frac{5}{4}\kappa_{TT}N_T^2\end{aligned}$$

$$\frac{dN_{SD}}{dt} = \kappa_{FRET} P_{0D} N_S + \frac{1}{4}\kappa_{TTD} N_{TD}^2 - (\kappa_{SD} + \kappa_{ISCD}) N_{SD}$$

(4)
$$- \left(\frac{7}{4}\kappa_{SSD} N_{SD} + \kappa_{SPD} N_P + \kappa_{STD} N_{TD} \right) N_{SD} - \xi P_{HO} (N_{SD} - W N_{0D})$$

(5)
$$\frac{d}{dt} N_{TD} = \kappa_{DEXT} P_{0D} N_T + \kappa_{ISCD} N_{SD} + \frac{3}{4}\kappa_{SSD} N_{SD}^2 - \kappa_{TD} N_{TD} - \frac{5}{4}\kappa_{TTD} N_{TD}^2 - \kappa_{TPD} N_{TD} N_P$$

(6)
$$\frac{d}{dt} P_{HO} = \beta_{sp}\kappa_{SD} N_{SD} + \left(\Gamma\xi (N_{SD} - W N_{0D}) - \kappa_{CAV} \right) P_{HO}$$

(7) $N_{0D} = N_{DOP} - N_{SD} - N_{TD}$

(8) $P_{0D} = \frac{N_{0D}}{N_{DOP}}$

where N_P is the polaron density, N_S the singlet and N_T the triplet population density, all in the host compound; N_{SD}, N_{TD}, and N_{0D}, are the respective dopant singlet, triplet and ground-state population densities. P_{HO} is the photon density, $J(t)$ the current density, d the active layer thickness and e the electron charge. Note that all densities in (2) to (8) are taken in the light-emitting layer. P_{0D} is the ratio of dopant ground-state molecules to the total number N_{DOP} of dopant molecules. W represents the overlap between the absorption spectrum $S_{ABS}(\lambda)$ and the electroluminescence spectrum $S_{EL}(\lambda)$ of the dopant,

(9) $$W = \frac{\int S_{ABS}(\lambda) S_{EL}(\lambda) S_{CAV}(\lambda) d\lambda}{\int S_{EL}^2 S_{CAV}(\lambda) d\lambda}$$

where $S_{CAV}(\lambda)$ is the cavity spectral shape. W accounts for the fraction of the dopant ground-state molecules that participate in the re-absorption of the emitted light. Note that W=1 for identical spectra, else $W < 1$.

A first remark concerns the light emission by the host singlet excitons (green in case of Alq3). As we will show in subsection J, the build-up of N_S remains relatively small, compared to N_{SD}. Moreover, no resonating structure is considered for the green light. Nevertheless, the host singlets will decay under spontaneous emission of green light. These emitted green photons are not considered in the rate equations.

As a second remark, note that the emission spectrum of an organic emitter is Stoke-shifted to the red by a few tens of nanometers from its absorption spectrum [14]. This implies that W will be quite small depending on the widths of the emission and absorption spectra. We estimate that in the weak micro-cavity limit with κ_{CAV}=3.0 × 10^{14} s^{-1}, we have $W \approx 0.026$, but as κ_{CAV} decreases with increasing cavity quality factor and the threshold for lasing is approached, the emitted spectrum will narrow dramatically, implying W to become much smaller. Therefore, W is a dynamical quantity and this will be studied in more detail in a future publication. Here, for the sake of simplicity, we will take W as a constant in the model. More about W will be discussed in subsection H. The values of the various parameters in (1) to (8) are given in table 1 and explained in detail in the next subsections A to G.

A. The polaron differential equation

Equation (1) describes the evolution of the polaron density with source term $J(t) / (e\, d)$, where e is the electron charge and d the thickness of the emitting layer. Polarons appear in two manifestations, positively charged hole-like polarons (density N_P^+) and negatively charged electron-like polarons (density N_P^-), where in view of assumed charge neutrality both populations are equal, $N_P^+ = N_P^-$. Moreover, each neutral polaron pair recombines to form one exciton and leave behind one neutral molecule which occurs at the Langevin-recombination rate γ [15]. This recombination process drives the electrical current and leads to the sink term in (1). In ref. 6 the value $\gamma = 6.2 \times 10^{-12}$ cm^3 s^{-1} is evaluated. An approximate expression for γ based on the Poole-Frenkel model shows an exponential dependence of the polaron mobilities to the electric field F related to the excitation current [16]

(10)
$$\gamma = \frac{e}{\epsilon}(\mu_h + \mu_e) \simeq \frac{e}{\epsilon}\mu_0 \exp\left(\frac{-E_a}{kT}\right)\exp\left(\frac{\delta\sqrt{F}}{kT}\right)$$

where ϵ is the dielectric constant, μ_h and μ_e are the respective hole and electron mobility, μ_0 is the trap-free charge mobility, E_a the activation energy, δ the Poole-Frenkel parameter, k the Boltzmann constant and T the temperature. In Alq3, the mobility of electrons is much larger than that of holes, therefore μ_h is neglected in first approximation [17]. According to (10) we expect the value of γ to increase exponentially with increasing applied diode voltage. For this reason, a larger value is expected at the high current densities (and thus high excitation voltage of 100V or above) needed to reach the laser threshold. Under such conditions γ has not been measured, but we will propose a better estimation below in subsection J, which is justified in sec.III. In the pulsed excitation regime, with the voltage being switched from zero to a maximum and back to zero, an on-off approximation is applicable and a fixed value for γ can be assumed, although a dynamical expression may be preferred in other types of excitation.

B. The host singlet-exciton equation

The first term on the right-hand side (r.h.s.) of (2) is a source for the singlet excitons coming from the above-mentioned polaron recombination term. The factor ¼ originates from the randomly injected spin statistics. The second term is a source term arising from triplet-triplet annihilation with generation rate κ_{TT} [13]. All other terms are sink terms.

The first sink term describes the Förster Resonance Energy Transfer (FRET) of singlet excitons from host to dopant molecules with a typical transfer time given by:

$$(11)\ \tau_{FRET} = \frac{1}{\kappa_{FRET}} = \tau_d \left(\frac{a}{R_0} \right)^6$$

where τ_d is the host (donor) exciton lifetime, R_0 is the Förster radius, and a is the average distance between the donor and the dopant (acceptor). It is approximated by half of the dopant molecule size,

$$(12)\ a = \frac{1}{2\sqrt[3]{N_{DOP}}}$$

where $N_{DOP} = C\, N_{MOL}$ is the molecular density of the guest (dopant), C its concentration and N_{MOL} the host density. In the case of the Alq3:DCM guest-host system, $\tau_d = 1 / \kappa_S = 12.5$ ns, $R_0 = 3.25$ nm, and $a = 1.43$ nm, the estimated transfer time is $\tau_{FRET} = 1/\kappa_{FRET} = 87\ ps$ and $\kappa_{FRET} = 1.15 \times 10^{10}\ s^{-1}$ [18, 19]. FRET is among the fastest mechanisms involved in the current dynamics and as such constitutes the most dominant sink term in (2). The probability P_{0D} accounts for the potential depopulation of the dopant ground state that would limit the energy transfer.

The second sink term describes the decay of the singlet exciton, modelled with the decay rate κ_S. This rate is related to the fluorescence lifetime which is known to be very sensitive to the environment and therefore subject to large uncertainties [20, 21]. Indeed, the singlet exciton lifetime of a neat Alq3 film measured under optical pumping was found to be between 12.5 ns and 20 ns [22, 23, 23, 25, 26]. We choose the singlet lifetime of Alq3 as $\tau_{PLAlq3} = 12.5$ ns, and calculate the host decay rate $\kappa_S = 8.0 \times 10^7\ s^{-1}$ [27]. The third sink term accounts for the non-radiative de-excitation mechanism, the inter-system crossing (ISC), which is a spin-flip-induced intra-molecular energy transfer from singlet to triplet with a decay rate κ_{ISC}. For Alq3 used as a host it is estimated to $2.2 \times 10^4\ s^{-1}$ in the literature [28]. The last sink terms in (2) describe the de-population of the host singlet density with different annihilation terms: singlet-singlet annihilation (SSA) with decay rate κ_{SS}, singlet-polaron annihilation (SPA) with decay rate κ_{SP}, and singlet-triplet annihilation (STA) with decay rate κ_{ST} [7, 13].

Table 1: Model parameters

Symbol	Name	Value	Ref.
S	OLED active area	10^{-4} cm^2	
d	OLED active layer thickness	380.0×10^{-9} m	
e	Charge of the electron	1.6×10^{-19} C	
γ	Langevin recombination rate	6.2×10^{-12} cm^3 s^{-1}	6
N_{MOL}	Molecular density	2.1×10^{21} cm^{-3}	
κ_{FRET}	Förster transfer rate	1.1×10^{10} s^{-1}	19
κ_S	Host singlet-exciton decay rate	8.0×10^7 s^{-1}	27
κ_{ISC}	Host inter-system crossing rate	2.2×10^4 s^{-1} to 1.0×10^7 s^{-1}	13, 28
κ_{SS}	Host singlet-singlet annihilation (SSA) rate	3.5×10^{-12} cm^3 s^{-1}	7
κ_{SP}	Host singlet-polaron annihilation (SPA) rate	3.0×10^{-10} s^{-1}	7,29
κ_{ST}	Host singlet-triplet annihilation (STA) rate	1.9×10^{-10} cm^{-3} s^{-1}	7
κ_{DEXT}	Dexter transfer rate	1.0×10^{10} s^{-1} to 5.0×10^{15} s^{-1}	30
κ_T	Host triplet decay rate	6.5×10^2 s^{-1} to 4.0×10^4 s^{-1}	7, 27
κ_{TP}	Host triplet-polaron annihilation (TPA) rate	2.8×10^{-13} cm^3 s^{-1}	7
κ_{TT}	Host triplet-triplet annihilation (TTA) rate	2.2×10^{-12} cm^3 s^{-1}	7
κ_{SD}	Dopant singlet-exciton decay rate	1.0×10^9 s^{-1}	7, 31, 32
κ_{ISCD}	Dopant inter-system crossing rate	2.2×10^4 s^{-1} to 1.0×10^7 s^{-1}	13, 28
κ_{SPD}	Dopant singlet-polaron annihilation (SPA) rate	3.0×10^{-10} cm^3 s^{-1}	7, 29
κ_{STD}	Dopant singlet-triplet annihilation (STA) rate	1.9×10^{-10} cm^3 s^{-1}	11
κ_{SSD}	Dopant singlet-singlet annihilation (SSA) rate	9.6×10^{-13} cm^3 s^{-1}	33
κ_{TD}	Dopant triplet decay rate	6.6×10^2 s^{-1}	34
κ_{TTD}	Dopant triplet-triplet annihilation (TTA) rate	2.4×10^{-15} cm^3 s^{-1}	28
κ_{TPD}	Dopant triplet-polaron annihilation (TPA) rate	5.6×10^{-13} cm^3 s^{-1}	9, 28
Γ	Confinement factor	0.29	
ξ	Stimulated emission gain coefficient	1.4×10^{-5} cm^3 s^{-1}	13
κ_{CAV}	Cavity photon decay rate	1-300 $\times 10^{12}$ s^{-1}	
β_{sp}	Spontaneous emission factor	$< 10^{-4}$ - 0.15	
C	Dopant concentration	2%	
N_{DOP}	Density of guest molecules	4.2×10^{19} cm^{-3}	

C. The host triplet-exciton equation

The rate equation (3) describes the variation of host triplet excitons. The first three terms in the r.h.s. are sources. The first is a contribution arising from the polaron recombination. With a 3/4 factor resulting from the spin statistics, this source term, when added to the first singlet source term in (2), matches the first sink term for the polaron recombination in (1). The second term describes the increase of N_T due to ISC in the same way as it decreases N_S in (2). The third term corresponds to the creation of triplets due to singlet-singlet absorption (SSA). The fourth term summarizes all decay processes respectively due to

Dexter transfer to dopant triplets, relaxation of the triplet excitons with decay time $\tau_T=1/\kappa_T$ [27] and triplet-polaron annihilation (TPA) [7]. Finally, the fourth term corresponds to triplet-triplet annihilation (TTA).

D. The dopant singlet-exciton equation

The dynamics of the dopant-singlet density N_{SD} is described by (4). The first term on the r.h.s. is the source as a result of the Förster energy transfer. This term matches the corresponding sink term in (2). With the exception of the last term on the r.h.s., all other terms are the corresponding counterparts of terms in (2).

In the first sink term, the dopant singlets decay radiatively at rate κ_{SD}. For the Alq3-DCM guest-host system we have taken the value $\kappa_{SD}=1.0 \times 10^9\ s^{-1}$ [7]. The last term describes the dopant singlet interaction with the photons due to stimulated emission with differential gain coefficient ξ. Here, the term $(N_{SD} - WN_{0D})$ is the effective inversion of the dopant singlets.

E. The dopant triplet-exciton equation

Rate equation (5) describes the dopant triplet density N_{TD} variations. The first term matches the corresponding Dexter transfer term in (3). The second term is the source resulting from the ISC matching the corresponding fourth term in (4). The third term represents the decay of the dopant triplet density at rate κ_{TD} by de-excitation, while other terms correspond to the absorption processes TTA (κ_{TTD}) and TPA (κ_{TPD}).

F. The photonic equation

Rate equation (6) accounts for the dynamics of the photon density P_{HO}. The first term on the r.h.s. gives the spontaneous-emission contribution arising from the radiative recombination of the dopant singlets N_{SD} at the rate κ_{SD} where the spontaneous-emission factor β_{sp} is the fraction of emitted photons within the lasing mode.

The second term gives the stimulated-emission net rate, where $(N_{SD} - W N_{0D})$ is the effective inversion, as also mentioned in section II.D. Γ is the confinement factor introduced to take into account the fact that only the part of the field wave-guided inside the gain medium is amplified. The last term on the r.h.s. accounts for the photon losses out of the cavity, with decay rate $\kappa_{CAV}=1/\tau_{CAV}$, where τ_{CAV} is the cavity photon lifetime. The net-amplification rate by stimulated emission is given by $A_{STIM}= \Gamma\xi(N_{SD} - WN_{0D})-\kappa_{CAV}$.

G. The optical gain

The optical gain per unit length is given by

$$(13)\quad g=\frac{n\xi}{c}N_{SD},$$

where n is the index of refraction in the material and c the light velocity. In optical pumping experiments, the gain is given in terms of slope coefficient K such that:

$$(14)\quad g=K I_P$$

where I_P is the optical pump intensity. With the photon flux nI_P / c, the equivalent excitation in terms of dopant-singlet excitons is

$$(15)\quad N_{SD}=I_P\frac{n\lambda_P}{hc^2}$$

where λ_P is the wavelength of the pump light and h the Planck's constant. Combining (13), (14) and (15), we obtain

$$(16)\quad \xi = \frac{c\,g}{n\,N_{SD}} = K\frac{hc^3}{n^2\lambda_P}.$$

This relates the gain parameter ξ to the slope coefficient K observed in optical pump experiments [12].

H. More about the W-factor

Despite the Stoke shift, the normalized absorption spectrum $S_{ABS}(\lambda)$ and the emission spectrum $S_{EL}(\lambda)$ of the emitted light by the dopant show some overlap, which induces a residual re-absorption of the light emitted by the dopant singlet excitons N_{SD}. With W representing the spectral overlap, (see [35]), the re-absorption rate per unit photon density equals $\Gamma\xi W N_{0D}$. Then, transparency is achieved when the available dopant singlet excitons N_{SD} precisely cancel the re-absorption, i.e,

$$(17)\quad N_{SD\ |\text{at transparency}} = W\,N_{0\,D}$$

Note that the re-absorption of photons yields a source term for the dopant singlet population in (4). In the bad-cavity limit, the reabsorption is maximal. When approaching the lasing threshold, the emission spectrum narrows, and W will become very small close to threshold and above.

I. Relation between the quality factor and cavity lifetime Tcav = $1/\kappa_{CAV}$

The losses resulting from the fraction of photons escaping the cavity per unit of time define a relationship between the cavity photon lifetime τ_{CAV} and the corresponding quality factor Q which reads:

$$(18)\quad Q = \omega_0\tau_{CAV},$$

where ω_0 is the resonance frequency of the cavity mode. The cavity photon decay rate κ_{CAV} can be expressed in the quality factor Q and the resonance wavelength in vacuum λ_0 as

$$(19)\quad \kappa_{CAV}=\frac{1}{\tau_{CAV}}=2\pi\frac{c}{n}\frac{1}{\lambda_0}\frac{1}{Q}.$$

At 620nm wavelength, a typical value for an OLED undergoing a parasitic weak microcavity effect is ($Q \sim 6$) corresponding to a cavity decay rate of $\kappa_{CAV} \approx 3.0 \times 10^{14}$ s^{-1}, and a photon life time in the cavity of $\tau_{CAV} \approx 3$ fs. A reasonable value for the quality factor $Q \approx 3000$ is achievable with a DFB-type of laser cavity and yields a cavity decay rate $\kappa_{CAV} \approx 5.4 \times 10^{11}$ s^{-1} corresponding to a photon life time of $\tau_{CAV} \approx 1.9$ ps.

J. Dynamical response to pulsed electrical excitation

The current model is used first to calculate the dynamical responses of OLEDs under intense electrical pulsed excitations in different configurations. More precisely, we calculate the polaron (N_P), host singlet and triplet (N_S, N_T), dopant singlet and triplet (N_{SD}, N_{TD}) and the photon (P_{HO}) densities as functions of time on the basis of equations (1) to (8). The excitation is modelled with an intense electrical pulse with sigmoid shape, duration of 20 ns, and rise time of 100 ps. We consider a high-speed 100×100 µm^2 ($S = 1.0 \times 10^{-4}$ cm^2) µ-OLED with an 80 nm thick organic heterostructure that incorporates an Alq3:DCM guest-host system with $\gamma = 1.3 \times 10^{-9}$ cm^{3}s^{-1} and other parameter values as in table 1.

The first case investigated is an OLED with a residual weak micro-cavity effect ($Q = 6$, $\kappa_{CAV} = 3.0 \times 10^{14}$ s^{-1}) and spectral overlap of $W = 2.6\%$. For this case, the peak current density is 3.25 kA/cm^2 and the dynamical responses are plotted in fig. 1.

Figure 1.a, shows the electrical current density $J(t)$ (blue solid line, left scale) and the polaron density N_P (cyan dash, right scale) as a function of time. We will discuss in the experimental section (§ III) the determining role of γ in the dynamics at the pulse onset.

Figure 1.b displays the host singlet N_S (green solid line) and triplet N_T (green dashes) densities. N_S increases with the pulse onset, reaches a first plateau at $\sim 1.5 \times 10^{17}$ cm^{-3} and increases again before reaching a second maximum at 2.5×10^{17} cm^{-3}. Note that the maximum triplet density is nearly two orders of magnitude larger than for the singlets. After the maximum the triplet density decays due to the non-radiative recombination (κ_T) and the Dexter transfer to the dopants (κ_{DEXT}).

The time evolution of the dopant singlet N_{SD} and triplet N_{TD} population densities are shown in fig. 1.c. N_{SD} (magenta solid line) increases quickly after the pulse onset, reaching a pronounced maximum at $\sim 7.5 \times 10^{17}$ cm^{-3} 3 ns after the pulse onset, and decreases shortly after that to reach a value of 5×10^{16} cm^{-3}, before vanishing after the end of the pulse. Note that N_{SD} at maximum is fivefold larger than the host-singlet maximum demonstrating a very efficient Förster transfer. Meanwhile N_{TD} (magenta dashes, right axis) increases steadily, reaches a plateau with a maximum $> 4.0 \times 10^{19}$ cm^{-3} and undergoes a very slow decay on a long (micro-second) time scale.

Figure 1.d presents the photon density P_{HO} (red solid line, right scale) and the net amplification (blue solid curve, left scale) as a function of time. P_{HO} increases quickly, and ~2 ns after the pulse onset it reaches a maximum at 3.7×10^{11}cm^{-3}, then decays to the value 2.5×10^{10} cm^{-3} until the end of the pulse and finally decays again.

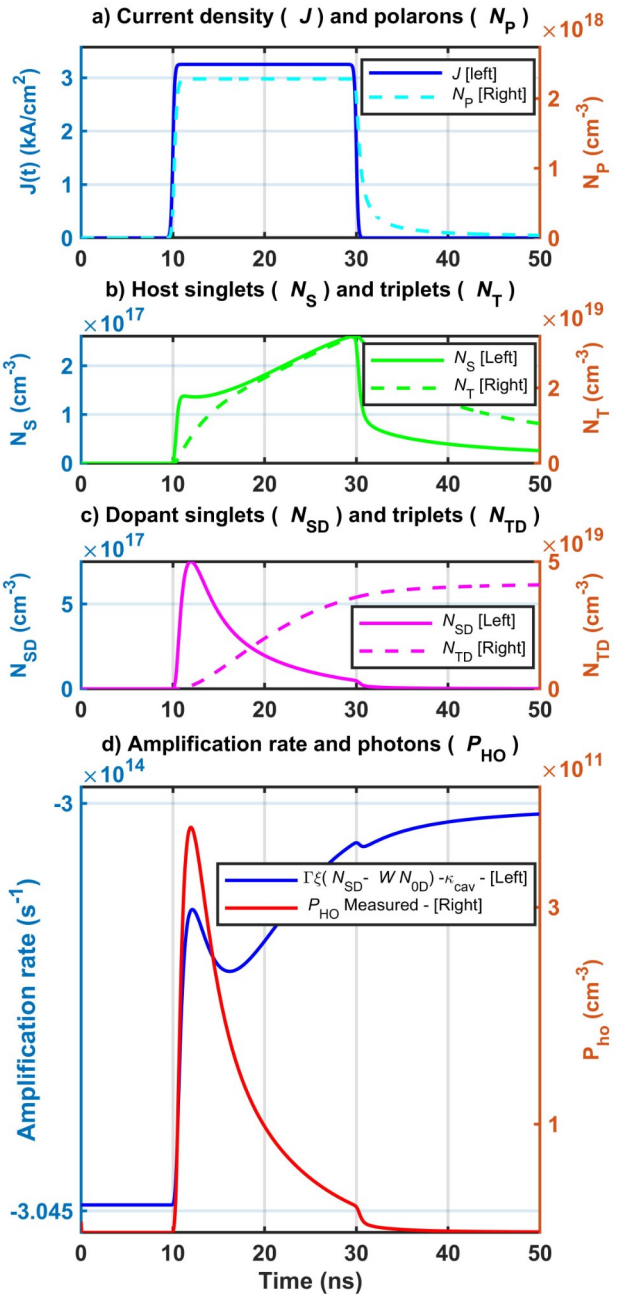

Figure 1: Dynamical response of a high-speed OLED with a weak microcavity effect submitted to a 20ns electrical pulse with intense current density (3.25 kA/cm^2), ($Q = 6$, $\kappa_{CAV} = 3.0 \times 10^{14}$ s^{-1}, $\gamma = 1.3 \times 10^{-9}$ cm^{3}s^{-1}, $\kappa_{DEXT} = 2.0 \times 10^{8}$ s^{-1}, $\kappa_{ISC} = \kappa_{ISCD} = 2.2 \times 10^{4}$ s^{-1}, $\kappa_T = 6.5 \times 10^{2}$ s^{-1}, $W = 2.6 \times 10^{-2}$, $\beta_{sp} = 0.15$.

As such, the photon density follows closely the singlet density which is a first strong indication that no laser action occurs. This is confirmed by the net-amplification rate (see sec. II.G) $A_{STIM} = \Gamma \xi \left(N_{SD} - W N_{0D} \right) - \kappa_{CAV}$ which remains large and negative. The net-amplification should climb up to a value close to zero if lasing is to be reached. The second case investigated consists of an OLED with a similar organic hetero-structure but with a high-quality factor micro-cavity ($Q = 1800$, $\kappa_{CAV} = 1.0 \times 10^{12}\ s^{-1}$), and a small spectral overlap $W = 0.0015$.

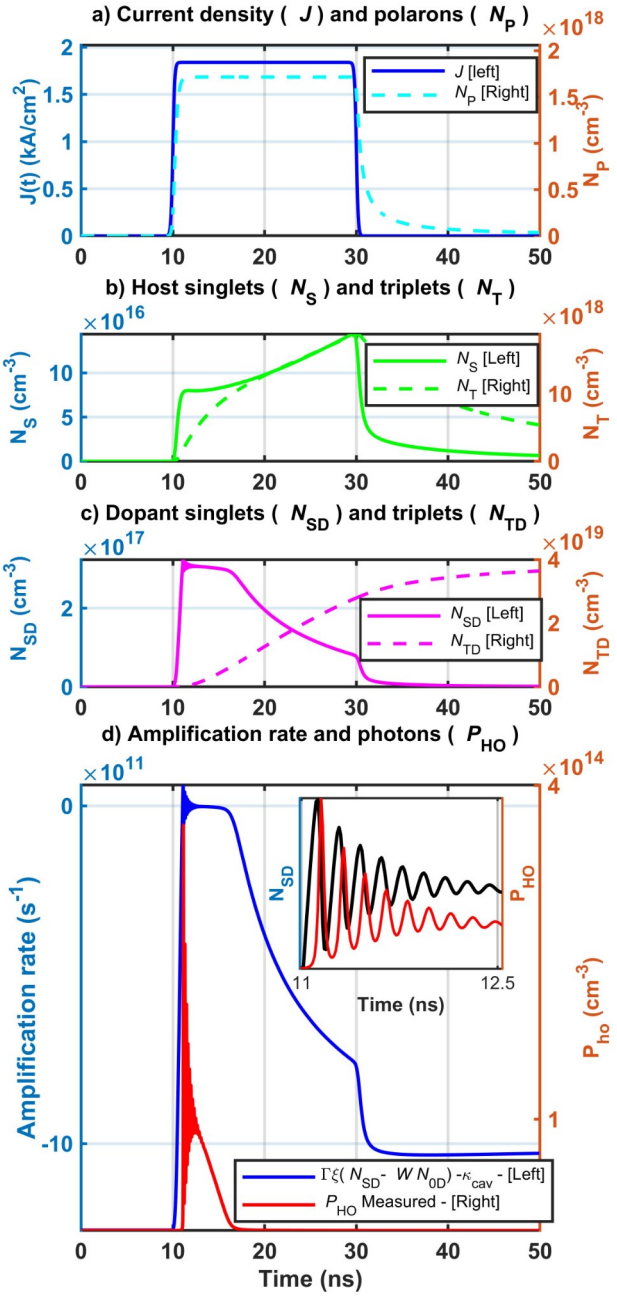

Figure 2: OLED with a high-quality factor Q=1800 microcavity, $k_{CAV} = 1.0 \times 10^{12}\ s^{-1}$, and peak current density $J = 1.84\ kA/cm^2$.$\gamma = 1.3 \times 10^{-9}\ cm^3\ s^{-1}$, $\kappa_{DEXT} = 2.0 \times 10^{8}\ s^{-1}$, $\kappa_{ISC} = \kappa_{ISCD} = 2.2 \times 10^{4}\ s^{-1}$, $\kappa_T = 6.5 \times 10^{2}\ s^{-1}$, $W = 1.5 \times 10^{-3}$ $\beta_{sp} = 5.0 \times 10^{-4}$. Inset shows an oscillation of photons in quadrature with that of the dopant-singlet density.

The dynamical responses calculated with a peak current density of $J = 1.84\ kA/cm^2$ are plotted in Fig. 2 with the same colour code as in Fig. 1.

Figure 2.a presents $J(t)$ and N_p versus time. In Fig. 2.b the host triplet N_T is seen to increase monotonously until the end of the pulse to $1.8 \times 10^{19}\ cm^{-3}$ which is more than 2 order of magnitude larger than the host singlet maximum ($1.4 \times 10^{17}\ cm^{-3}$). It decays very rapidly afterwards.

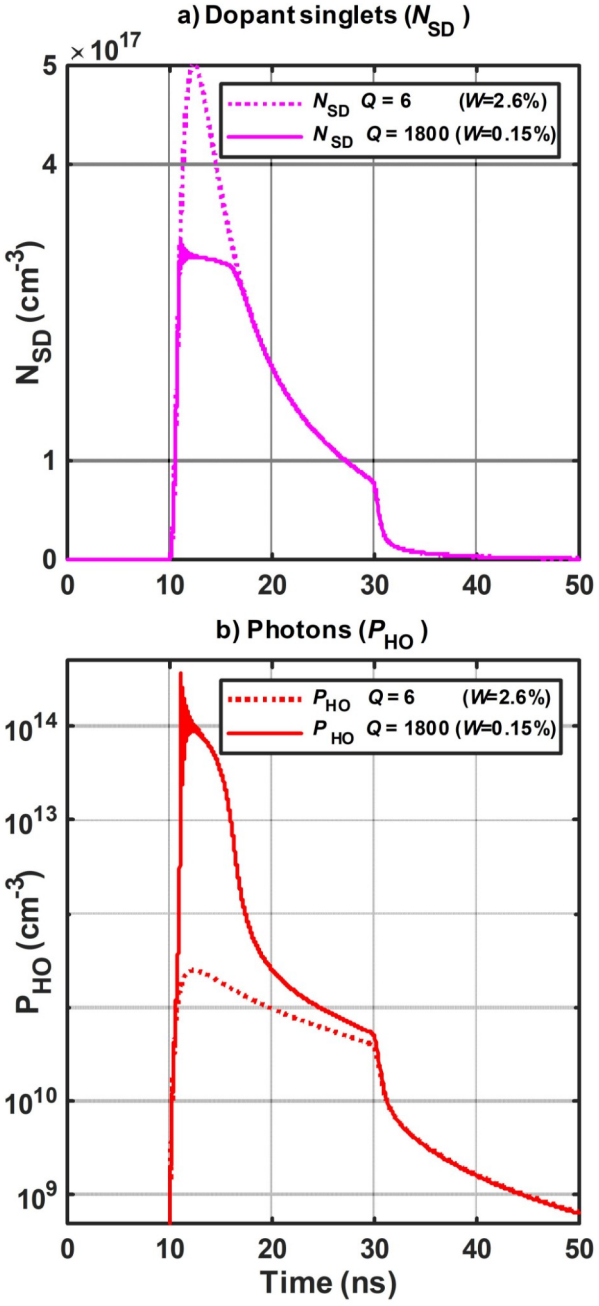

Figure 3: Comparison between spontaneous and stimulated emission high-lighting the signatures of lasing. a) Singlet densities versus time for the low-Q micro-cavity (magenta dotted line) and high-Q micro-cavity (magenta solid line). Note the clamping of N_{SD} in the high-Q case. b) Photon densities versus time for the low-Q (red dotted line) and high-Q micro-cavity (red solid line). Note the logarithmic scale.

In Fig. 2.c the dopant singlets N_{SD} increase sharply to a maximum of 3.0×10^{17} cm^{-3}, reached 1.1 ns after the pulse onset, where it clamps for another 2ns before it decays slowly until the end of the pulse and then decays quickly again. The maximum of N_{SD} is somewhat smaller than in the previous case of Fig. 1, as a consequence of the clamping, a first indication of lasing.

In Fig. 2.d, the photon density starts with a steep rising flank, reaches a sharp maximum of 3.6×10^{14} cm^{-3}, 1.1 ns after the beginning of the pulse and shows a damped GHz oscillation followed by a fast decay. The photon-density peak is three orders of magnitude larger than in the OLED case of Fig. 1.d for a smaller current density. The net-amplification rate rises from -1.2×10^{12} s^{-1} up to a positive value ($+6.1 \times 10^{10}$ s^{-1}) before slowly decaying during the excitation pulse down to -1.0×10^{12} s^{-1}. The positive value means that amplification of the light is taking place while the dopant exciton population clamps at its threshold value. This is a demonstration of lasing.

Note that the oscillations of the photon density become less damped when the electrical injected pulse amplitude increases. The inset of Fig. 2.d. exhibits 6 GHz photon oscillations in quadrature with the oscillation of N_{SD}. Such oscillations in the light intensity are typical for lasers described by two or more coupled rate-equations and are called relaxation oscillations [36]. For this reason, and on the basis of the proposed model, we predict the existence of GHz relaxation oscillations in OLDs lying at the origin of a large variety of dynamical behaviours similar to conventional semiconductor diode lasers [36].

In order to highlight the difference between spontaneous and stimulated emissions, fig.3 shows the net-amplification rate and photon density versus time for both the weak micro-cavity OLED case ($Q = 6$) of fig. 1and the high-Q micro-cavity case ($Q = 1800$) of fig. 2. Three signatures of the lasing mechanism can be identified. Firstly, the clamping of N_{SD} occurs during the maximum of emission for the high-Q case (magenta line) and not for the low-Q case (magenta dots) (fig. 3.a). Secondly, the increase from a negative to a positive value close to zero of the net-amplification only occurs in the high-Q cavity case (blue solid line in fig.2.d). A third signature of lasing is the dramatic increase in the photon density by more than 3 orders of magnitude illustrating the difference between lasing (red solid line) and spontaneous emission (red dots) as shown in fig. 3.b.

III. Experimental results

The reliability and relevancy of the model is checked by confronting the dynamical response of the model with experimental results. More precisely, the objective is to compare the calculated dynamics of the photon density with the measured optical response of an OLED under similar pulsed electrical excitation.

A. High speed OLED fabrication

The first considered high-speed organic hetero-structure (OLED 1) has been deposited on a co-planar waveguide electrode etched on ITO coated glass substrate, similar to what was reported in previous work, but with local gold metallization to reduce the serial resistances to $R_{s1} = 43\ \Omega$ and with a measurement resistance of R_{meas1}=13 Ω and a parasitic capacitance of $C = 4.2$pF. The resulting electrical time constant at $V = 0$ (Dynamical resistance is infinite) is $\tau_{RC} = 225$ ps [31, 37, 38]. The organic hetero-structure of OLED 1 consists of 30nm of m-MTDATA (*4,4',4"-Tris (N-3-methylphenyl-N-phenyl-amino)triphenylamine*) as hole injection layer (HIL), 10 nm-thick NPD (*N, N'-Di (1-naphthyl-N, N'-diphenyl-(1,1'-biphenyl)-4,4'diamine*) as hole transporting layer (HTL), 30 nm of Alq3 (*tris(8-hydroxyquinoline)aluminum*) doped with DCM (*(E)-2-(2-(4-(dimethylamino)styryl)-6-methyl-4H-pyran-4-ylidene)malononitrile*) as light emitting layer, 5nm of BCP (*2,9-Dimethyl-4,7-diphenyl-1,10-phenanthroline*) as hole blocking layer (HBL), 25 nm of Alq3 as electron transporting layer, and a final cathode layer of LiF(1nm)/Al (120nm).

In a second sample (OLED 2), the organic hetero-structure consists of 35nm of m-MTDATA (HIL), 15 nm of NPD (HTL), 30 nm of Alq3 doped with 2% of DCM as light emitting layer, 5nm of TPBi (*2,2',2"-(1,3,5-Benzinetriyl)-tris(1-phenyl-1-H benzimidazole*) as HBL, 25 nm of Alq3 as electron transporting layer, and a final cathode layer of LiF (1nm) / Al (120 nm). The serial resistances is reduced to $R_{s2} = 23\ \Omega$. and its built-in measurement resistance has been reduced from $R_{meas} = 13\ \Omega$ το $R_{meas2} = 4\ \Omega$. The active area has been reduced to $S_2 = 100\ \mu m \times 50\ \mu m$ resulting in a reduction of the capacitance to 1.3 pF. The resulting electrical time constants at 0V is $\tau_{RC2} = 35$ps.

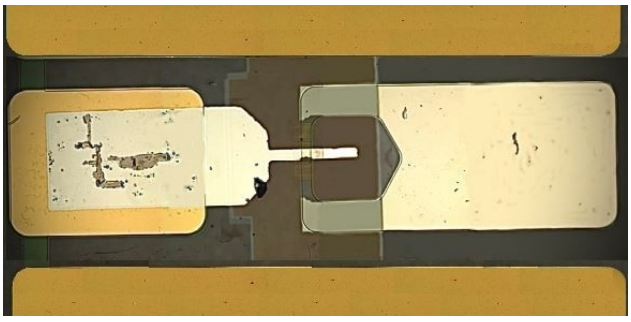

Figure 4: Top view of OLED 2 deposited on gold metallized coplanar waveguide electrodes.

These structures are deposited by thermal evaporation using hollow silicon mask. The deposition rates and the thickness are monitored by quartz sensors. A top view of a typical sample is presented in fig. 4.

The measurement system consists of a probe station (Cascade PM5), a high pulse generator (AVTECH AVL-2A-B), a digital oscilloscope (Tektronix TDS 6604), an avalanche photodiode (Thorlabs APD 430A2), a CCD camera and a spectrophotometer (Horiba Scientific IHR550) coupled to a streak camera (Optronis). This system enables simultaneous measurements of the electrical injection current density, the emitted light intensity and its time-resolved spectrum of the device under single shot excitations.

The optical measurement system has been calibrated with a calibrated source. All measurements are realized in ambient atmosphere at room temperature.

B. Comparison between calculated response and experimental results

A 20 ns, 45 V (respectively 43V) pulse excitation voltage is applied to the OLED 1 (respectively OLED 2) and the electrical injection current is measured and recorded together with the emitted light intensity. The measured current is taken as the source term in the polaron rate equation (1).

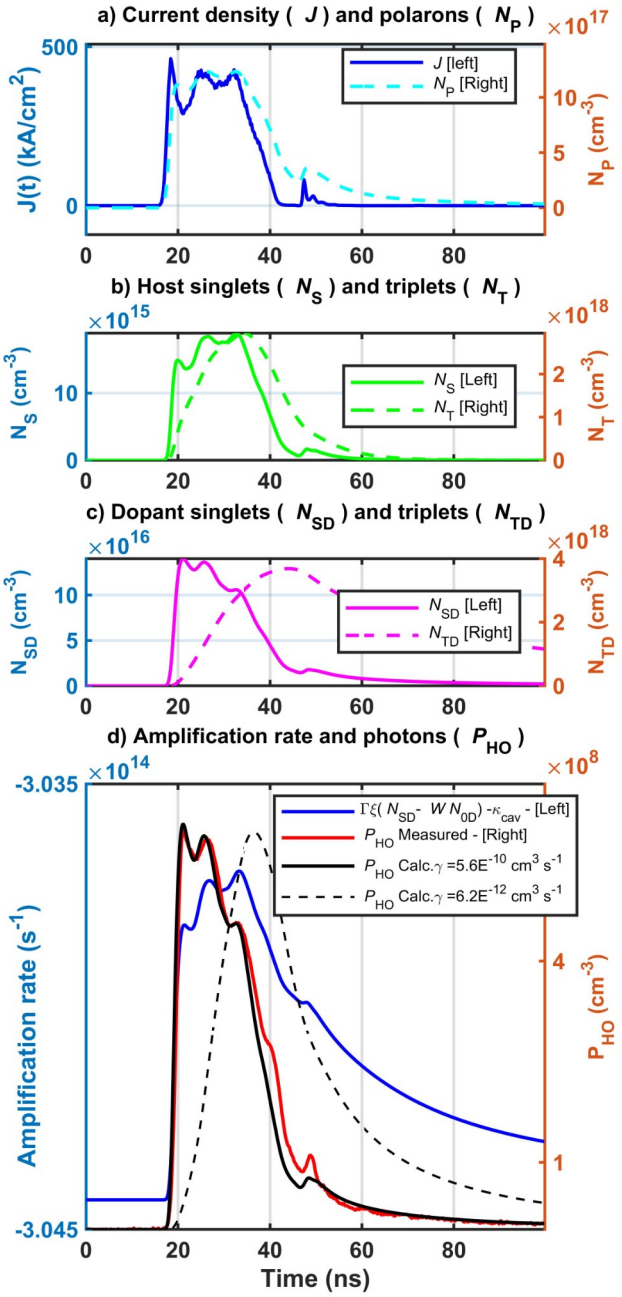

Figure 5: Comparison between measurements and simulation of the dynamical optical responses of a CPW OLED under a peak current density of 0.462 kA/cm². The parameters are fine tuned as in Table 2 (OLED 1).

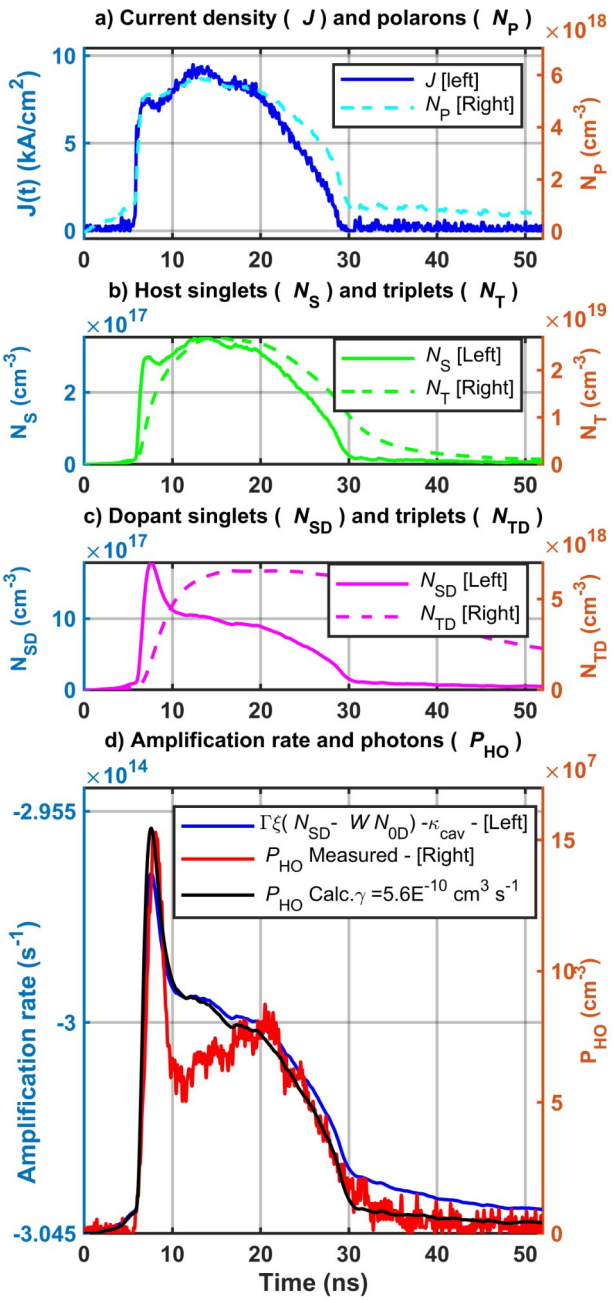

Figure 6: Comparison between measured and calculated optical response of a CPW OLED under a current density of 8.8 kA/cm². The parameters are fine tuned as in table 2 (OLED 2).

The photon density is then calculated from the set of equations (1)-(8) with the model parameters listed in Table 2, which have been fine tuned for fitting purpose. The resulting calculated population densities are then plotted in Fig. 5 and Fig. 6, together with the measured and calibrated optical response of the OLED for comparison.

Figure 5.a shows the effective current density (dark blue solid line) peaking at 0.45 kA / cm^2, calculated according to a previously developed equivalent electrical model [38], and from which the polaron density is calculated according to Eq. (1) (light blue dashed). The calculated respective singlet and triplet host populations are plotted in Fig. 5.b respectively with a green solid line and a dashed lines. The dopant singlet (magenta solid line) and triplet density (magenta dashes) are plotted in Fig. 5.c.

Table 2: Model parameters used to simulate experiment

Symbol	OLED 1	OLED 2
S	1.5×10^{-4} cm^2	0.5×10^{-4} cm^2
d	30×10^{-7} cm	30×10^{-7} cm
γ	5.6×10^{-10} cm^3 s^{-1}	5.6×0^{-10} cm^3 s^{-1}
κ_S	8.3×10^{7} s^{-1}	8.3×10^{7} s^{-1}
κ_T	6.5×10^{2} s^{-1}	6.5×10^{2} s^{-1}
κ_{SP}	1.0×10^{-11} cm^3 s^{-1}	1.0×10^{-11} cm^3 s^{-1}
κ_{ST}	2.5×10^{-10} cm^{3}s^{-1}	2.5×10^{-10} cm^{3}s^{-1}
κ_{FRET}	1.15×10^{10} s^{-1}	1.15×10^{10} s^{-1}
κ_{ISC}	2.2×10^{4} s^{-1}	2.2×10^{4} s^{-1}
κ_{DEXT}	2.0×10^{8} s^{-1}	2.0×10^{8} s^{-1}
κ_{TP}	2.8×10^{-13} cm^{3}s^{-1}	2.8×10^{-11} cm^{3}s^{-1}
κ_{TT}	2.2×10^{-12} cm^{3}s^{-1}	5.5×10^{-12} cm^{3}s^{-1}
κ_{SS}	3.5×10^{-12} cm^{3}s^{-1}	3.5×10^{-12} cm^{3}s^{-1}
κ_{SSD}	9.6×10^{-13} cm^{3}s^{-1}	9.6×10^{-13} cm^{3}s^{-1}
κ_{SD}	1.0×10^{9} s^{-1}	1.0×10^{9} s^{-1}
κ_{ISCD}	2.2×10^{4} s^{-1}	2.2×10^{4} s^{-1}
κ_{SPD}	3.0×10^{-11} cm^{3}s^{-1}	3.0×10^{-11} cm^{3}s^{-1}
κ_{STD}	3.7×10^{-10} cm^3 s^{-1}	3.7×10^{-10} cm^3 s^{-1}
κ_{TD}	6.6×10^{2} s^{-1}	6.6×10^{2} s^{-1}
κ_{TTD}	8.0×10^{-12} cm^{3}s^{-1}	2.0×10^{-11} cm^{3}s^{-1}
κ_{TPD}	9.0×10^{-11} cm^3 s^{-1}	9.0×10^{-11} cm^3 s^{-1}
ξ	1.4×10^{-5} s^{-1}	1.4×10^{-5} s^{-1}
κ_{cav}	3.0×10^{14} s^{-1}	3.0×10^{14} s^{-1}
β_{sp}	1.3×10^{-3}	2.6×10^{-4}
W	2.6×10^{-2}	2.6×10^{-2}

Figure 5.d shows the net-amplification (blue solid line), the measured photon response (red solid line), the photon density calculated with the fine tuned $\gamma_1 = 5.6 \times 10^{-10}$ cm^3 s^{-1} (solid black line) and with the literature value $\gamma_2 = 6.2 \times 10^{-12}$ cm^3 s^{-1} (black dashed line). The simulation with γ_1 clearly shows a very good qualitative agreement with the measurement especially for the rising flank, the top of the pulse and the far tail. However with γ_2 no agreement can be achieved. Clearly, in this high current density and nanosecond regime, the literature value of the Langevin recombination rate ($\gamma_2 = 6.2 \times 10^{-12}$ cm^{3}s^{-1}) is too small to explain both the slope of the rising flank and the tail of the pulse of the photon response as shown in Fig. 5.d. The fitted value $\gamma_1 = 5.6 \times 10^{-10}$ cm^3 s^{-1} is nearly 2 orders of magnitude larger. We attribute this to the exponential dependence of the mobility on the square root of the electric field expressed in (10). The fact that the model is able to reproduce qualitatively the optical response of an OLED on the basis of the same excitation current density signal is a strong indication of the validity of the model.

Next, the calculated dynamics of the photon density is compared with the measured optical response under higher pulsed current density of OLED 2.

The polaron, singlet, triplet and photon densities are calculated with the fine-tuned parameters presented in the third column of Table 2 and are plotted in Fig. 6. Figure 6.a exhibits a current density approaching 10 kA/cm^2 (8.8 kA/cm^2), resulting in a polaron density maximum of 5.5×10^{18} cm^{-3}. The maxima of host and dopant singlet densities in Figs. 6.b and 6.c are respectively 3.5×10^{17} cm^{-3} and 1.7×10^{18} cm^{-3}. Fig. 6.d presents the calculated (black) and measured photon density (red) which exhibit less agreement compared to the first experiment, specifically during some 10 ns directly following the peak.

We believe this less satisfactory fit in the ultra-high current density case is due to the higher current density, leading to less uniform spatial distribution of the polarons within the organic layers. Taking into account such spatial dependence is beyond the scope of this paper.

Nevertheless, with these experimental validations laser threshold predictions can be made.

IV. Threshold estimation

The laser threshold will be estimated for the Alq3:DCM guest-host system for two different gain values. The first is for $\xi_1 = 1.4 \times 10^{-5}$ cm^3 s^{-1} as in Table 1 and 2 and the second for $\xi_2 = 4.8 \times 10^{-6}$ cm^3 s^{-1}, a gain value similar to that of BsB-Cz (*4,4'-bis[(N-carbazole)styryl]biphenyl*), which is the gain medium in the experiment reported by Adachi's group [1]. Although BsB-Cz is not a guest-host system, Förster transfer is so fast (87 ps) that we assume in lowest approximation the guest to be "transparent". In both cases all other model parameters are those given in Tables 2, column 2 for OLED 1 except $\kappa_{ST} = 1.0 \times 10^{-12}$ cm^3 s^{-1} and $\kappa_{STD} = 1.0 \times 10^{-12}$ cm^3 s^{-1}. The amplitude of the sigmoid shaped pulsed current density is varied from 0.1 kA/cm^2 to 10 kA/cm^2 close to the maximum current density achieved in this study. For each of the applied current amplitudes, we integrate the photon densities over the pulse duration.

Figure 7 displays the calculated L-I curves in a log-log plot for 4 different values of the Q-factor, $Q_1 = 1{,}000$ (black), $Q_2 = 3{,}000$ (dark blue), $Q_3 = 10{,}000$ (light blue), $Q_4 = 30{,}000$ (green) and

two different values for W (i.e. $W_1 = 1.5 \times 10^{-3}$ (dashes) and $W_2 = 0$ (solid lines)). Figure 7.a shows the first case (Alq3:DCM as gain medium; parameters as in Table 2) while Figure 7.b presents the second case with a gain coefficient equal to that of BsB-Cz and reduced singlet-triplet absorption $\kappa_{ST} = 1.0 \times 10^{-12}$ cm^3 s^{-1} and $\kappa_{STD} = 1.0 \times 10^{-12}$ cm^3 s^{-1} [1]. The S-shaped curves in log-log scale are typical of laser characteristics. The laser threshold current is defined as the inflexion point of the L-I curve.

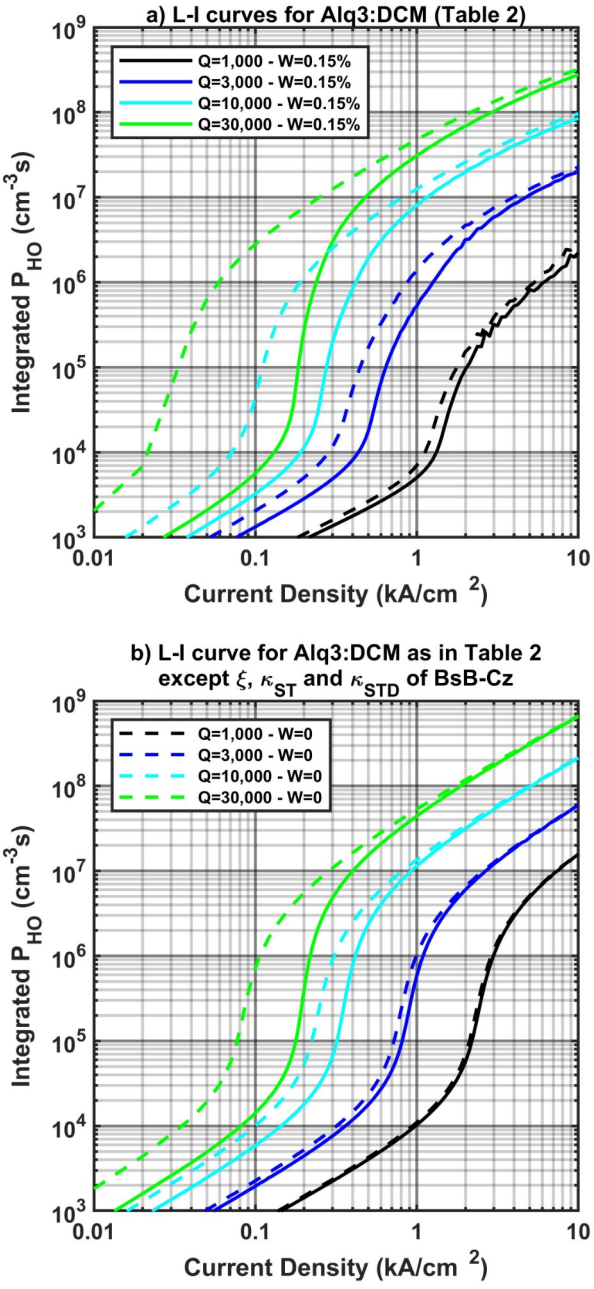

Figure 7: Light-current curve as a function of the quality factor for different gain media. a) Gain medium is Alq3:DCM guest-host system with $\xi_1 = 14 \times 10^{-6}$ cm^3 s^{-1}. b) Gain coefficient $\xi_2 = 4.8\ 10^{-6}$ cm^3 s^{-1}, $\kappa_{ST}=1\times10^{-12}$ cm^3 s^{-1}, $\kappa_{STD}=1\times10^{-12}$ cm^3 s^{-1} as for BsB-Cz [1]. Solid lines are with $W_1 = 1.5\ 10^{-3}$ and dashed lines with $W_2 = 0$.

In the first case, with $W_1 = 1.5 \times 10^{-3}$ the laser thresholds are estimated as $J_{th4\_1} = 0.18$ kA/cm^2 for $Q_4 = 30{,}000$; $J_{th3\_1} = 0.28$ kA/cm^2 for $Q_3 = 10{,}000$; $J_{th2\_1} = 0.63$ kA/cm^2 for $Q_2 = 3{,}000$ and J_{th1_1} is predicted 1.78 kA/cm^2. With $W = 0$, the threshold currents are lower with $J_{th4\_0} = 0.04$ kA/cm^2 for $Q_4 = 30{,}000$; $J_{th3\_0} = 0.11$ kA/cm^2 for $Q_3 = 10{,}000$; $J_{th2\_0} = 0.44$ kA/cm^2 for $Q_2 = 3{,}000$, while $J_{th1\_0} = 1.58$ kA/cm^2. We recall the significance of W (see Sec, IIH). Above threshold $W \sim 0$, whereas below threshold a value >0 applies. Hence, the real threshold will lay somewhere between the two values obtained for each Q. In Fig. 7.b, for $W = 1.5 \times 10^{-3}$ (solid curves), the respective thresholds are $J_{th4} = 0.19$ kA/cm^2, $J_{th3} = 0.36$ kA/cm^2, $J_{th2} = 0.89$ kA/cm^2 and $J_{th1} = 2.37$ kA/cm^2.

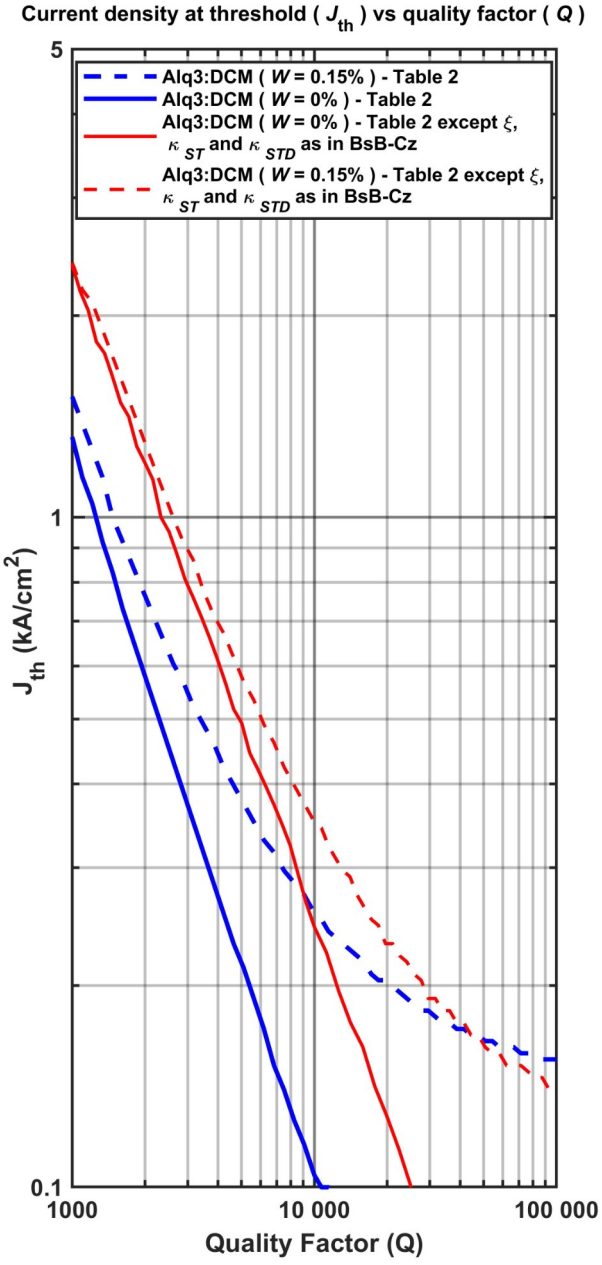

Figure 8: Threshold current density as a function of the quality factor Q for the two cases of Fig. 7.a and 7.b.

With $W = 0$ (dashed curves), the threshold currents are lower with $J_{th4} = 0.08$ kA/cm^2, $J_{th3} = 0.25$ kA/cm^2, $J_{th2} = 0.8$ kA/cm^2 and $J_{th1} = 2.35$ kA/cm^2.

As a first conclusion, we obtain a laser threshold as low as 0.54 kA/cm^2 with a gain coefficient equal to that of BsB-Cz as gain medium and for the smaller values for $\kappa_{ST(D)}$ (1×10^{-12} cm^{3}s^{-1} [39]), like in the experiment of Adachi's group, provided that the quality factor is in the range $3{,}000 < Q < 10{,}000\sim$ and without residual absorption ($W = 0$).

To investigate further this finding, we show in Fig. 8 a log-log plot of the threshold current density as a function of the quality factor for two values of W, i.e. 1.5×10^{-3} (dashed line) and 0 (solid line) Red curves are for $\xi_1 = 1.4 \times 10^{-5}$ s^{-1} (Alq3:DCM) and blue curves for $\xi_2 = 4.8 \times 10^{-6}$ s$^{-1.}$ (BsB-Cz). Obviously, these curves confirm the decrease of the threshold current density with the increase of the quality factor Q.

Two different types of decreasing functions can be distinguished. For $W_2 = 0$, the functions (blue and red solid lines) show a continuous linear decrease (in log-log scale), whereas for $W_1 = 1.5 \times 10^{-3}$ (red and blue dashed lines) the function exhibits a saturation towards 0.13-0.15 kA/cm^2. This saturation occurs when the residual absorption loss annihilates the benefice of a higher quality factor. From Fig. 8, one can identify more precisely the conditions to obtain a threshold current density as low as 0.54 kA/cm^2.: In the first case, with Alq3:DCM as a gain medium, the quality factor is to exceed $Q_1 \sim 2{,}100$ with $W = 0$, and $Q_1 \sim 3.100$ with $W_1 = 1.5 \times 10^{-3}$. In the second case, with BSB-Cz gain value and reduced STA, the quality factor is to exceed $Q_2 \sim 4{,}300$ with no residual absorption ($W = 0$) and $Q_2 \sim 5{,}500$ for $W_1 = 1.5 \times 10^{-3}$.

V. Conclusion

We have established a new model based on rate equations for the dynamics of the spontaneous and stimulated emission of a red emitting OLD. The model, which is also valid for OLEDs with small quality factors, takes account of the guest-host system, where the host-singlet excitons form a reservoir from which the dopant-singlet excitons are delivered. A key parameter W was introduced to take into account the residual absorption resulting from the partial overlapping of the (broad) absorption and (narrow) emission spectra.

On the basis of the proposed model, we simulate the dynamical responses of different OLEDs to a sigmoid-like pulsed electrical excitation with a duration of 20ns and various peak current amplitudes. The calculated time responses include the population densities of polarons, of host singlets and triplets, of dopant singlets and triplets, and of photons. The dynamical behaviours of OLEDs in a low-Q cavity on the one hand and in a high-Q cavity with $Q = 1{,}800$, on the other hand, are simulated and compared.

The predicted optical response of the high-Q OLED exhibits (a) a sudden dramatic increase of the photon density for a duration much smaller than that of the electrical excitation with (b) a damped oscillation in the GHz regime and (c) clamping behaviour for the dopant-singlet density. This is reminiscent of laser action and leads us to predict the existence of relaxation oscillations in OLDs very similar to those reported and extensively studied in conventional III-V laser diodes [36].

The comparison between OLED and OLD highlights three signatures of the lasing phenomenon. Firstly, the optical response after the pulse onset is orders of magnitude larger in the laser case than in the OLED case. Secondly the dopant singlet density is clamped during the lasing action and, thirdly, the sign of the net-amplification changes from negative to positive. The model is validated by comparing the calculated optical response with the measured light emission, first in an experiment where a high-speed low-Q OLED (OLED 1) is submitted to a 20 ns electrical pulse with current density of 0.4 kA/cm^2. The very good agreement confirms the validity and the relevancy of the model. Measurements with another OLED (OLED 2), applied to a much higher current density reaching 8.8 kA/cm^2, turn out to be more difficult to fit to the simulations, presumably due to spatial inhomogeneities induced by the high current density, which might affect the polaron distribution.

This has to be investigated further. One reason to present Fig. 6 is to demonstrate that the current of 10 kA/cm^2, that was used as an upper limit in Figs. 7 and 8, is experimentally reachable.

On the basis of the validated model, the light-current curves have been calculated for different values of the quality factor, and for two different organic gain media, ie Alq3:DCM and BsB-Cz. On the basis of the parameter set used for Fig. 2 and with $\xi_2 = 4.8 \times 10^{-6}$ cm^3 s^{-1}, we predict for the latter organic compound a laser threshold as low as 0.54 kA cm^{-2} if the quality factor is taken as $Q = 4{,}300$ and provided that there is no residual absorption ($W = 0$). Therefore, the model confirms the possibility of the threshold-current density of 540 A/cm^2 observed in the recent first experimental indication of lasing in an OLED [1].

Finally, as a guide-line for the fabrication of OLDs, we show the predicted laser threshold as a function of the quality factor for different configurations.

This work is intended to bridge the gap between the communities of organic chemistry, material sciences and laser dynamics in order to gather and strengthen wider expertise in the emerging field of organic laser diode.

VI. Acknowledgment

This work was supported by the French Agence Nationale de la Recherche through the Program Investissement d'Avenir under Grant ANR-11-IDEX-0005-02, by the Labex SEAM: Science Engineering and Advanced Materials,

VII. References

[1] A. S. D. Sandanayaka et al., "Indication of current-injection lasing from an organic semiconductor," Appl. Phys. Express, vol. 12, no. 6, p. 061010, May 2019, doi: 10.7567/1882-0786/ab1b90

[2] F. Torricelli and L. Colalongo, "Unified Mobility Model for Disordered Organic Semiconductors," *IEEE Electron Device Lett.*, vol. 30, no. 10, pp. 1048–1050, Oct. 2009, doi: 10.1109/LED.2009.2027998.

[3] Murgatroyd, P. N. Theory of space-charge-limited current enhanced by Frenkel effect. *J. Phys. D: Appl. Phys.***3**, 151–156 (1970). 10.1088/0022-3727/3/2/308

[4] M. Osinski and J. Buus, "Linewidth broadening factor in semiconductor lasers–An overview," *IEEE Journal of Quantum Electronics*, vol. 23, no. 1, pp. 9–29, Jan. 1987, doi: 10.1109/JQE.1987.1073204.

[5] J. L. Segura, "The chemistry of electroluminescent organic materials," Acta Polymerica, vol. 49, no. 7, pp. 319–344, 1998, doi: 10.1002/(SICI)1521-4044(199807)49:7<319::AID-APOL319>3.0.CO;2-Q.

[6] C. Gartner, C. Karnutsch, C. Pflumm, and U. Lemmer, "Numerical Device Simulation of Double-Heterostructure Organic Laser Diodes Including Current-Induced Absorption Processes," IEEE Journal of Quantum Electronics, vol. 43, no. 11, pp. 1006–1017, Nov. 2007, doi: 10.1109/JQE.2007.905021.

[7] D. Kasemann, R. Brückner, H. Fröb, and K. Leo, "Organic light-emitting diodes under high currents explored by transient electroluminescence on the nanosecond scale," Phys. Rev. B, vol. 84, no. 11, p. 115208, 2011, doi: 10.1103/PhysRevB.84.115208.

[8] S.-L. Chua, B. Zhen, J. Lee, J. Bravo-Abad, O. Shapira, and M. Soljačić, "Modeling of threshold and dynamics behavior of organic nanostructured lasers," J. Mater. Chem. C, vol. 2, no. 8, pp. 1463–1473, Jan. 2014, doi: 10.1039/C3TC31870B.

[9] V. Ahmad, J. Sobus, M. Greenberg, A. Shukla, B. Philippa, A. Pivrikas, G. Vamvounis, R. White, S.-C. Lo, and E.B. Namdas, Nat Commun **11**, 4310 (2020).

[10] A. A. Shoustikov, Yujian You, and M. E. Thompson, "Electroluminescence color tuning by dye doping in organic light-emitting diodes," IEEE J. Select. Topics Quantum Electron., vol. 4, no. 1, pp. 3–13, Feb. 1998, doi: 10.1109/2944.669454.

[11] N.C. Giebink and S.R. Forrest, "Temporal response of optically pumped organic semiconductor lasers and its implication for reaching threshold under electrical excitation", Physical Review B 79, 073302, 2009. 10.1103/PhysRevB.79.073302

[12] I. Gozhyk, "Polarization and gain phenomena in dye-doped polymer micro-lasers", Thesis Ecole normale superieure de Cachan (F), 2012

[13] C. Gaertner, "Organic Laser Diodes: Modelling and Simulation", Thesis Universitaet Karlsruhe (D), 2008

[14] J. R.Gispert, Coordination Chemistry. (2008). Wiley-VCH. p. 483. ISBN 3-527-31802-X https://doi.org/10.1002/aoc.1550

[15] P. Langevin, Ann. Chim. Phys. 28,433,1903

[16] Kao, K. C. Dielectric Phenomena in Solids; Elsevier Academic Press: San Diego, 2004. Hardcover ISBN: 9780123965615

[17] P. Juhasz, J. Nevrela, M. Micjan, M. Novota, J. Uhrik, L. Stuchlikova, J. Jakabovic, L. Harmatha and M. Weis, "Charge injection and transport properties of an organic light-emitting diode," Beilstein J. Nanotechnol., vol. 7, no. 1, pp. 47–52, Jan. 2016, doi: 10.3762/bjnano.7.5.

[18] N. Tsutsumi and T. Hinode, "Tunable organic distributed feedback dye laser device excited through Förster mechanism," Appl. Phys. B, vol. 123, no. 3, p. 93, Mar. 2017, doi: 10.1007/s00340-017-6679-x.

[19] V. G. Kozlov, V. Bulovic, P.E. Burrows, M. Baldo, V.B. Khalfin, G. Parthasaraty, S.R. Forrest, Y. You, E. Thompson., "Study of lasing action based on Förster energy transfer in optically pumped organic semiconductor thin films," J. Appl. Phys., vol. 84, no. 8, p. 14, 2014. doi.org/10.1063/1.368624

[20] U. Noomnarm and R. M. Clegg, "Fluorescence lifetimes: fundamentals and interpretations," Photosynth Res, vol. 101, no. 2–3, pp. 181–194, Sep. 2009, doi: 10.1007/s11120-009-9457-8.

[21] M. A. Omary and H. H. Patterson, "Luminescence, Theory," in *Encyclopedia of Spectroscopy and Spectrometry*, Elsevier, 2017, pp. 636–653. DOI: 10.1016/B978-0-12-803224-4.00193-X

[22] C.W. Tang, S.A. VanSlyke, C.H. Chen, J. Appl. Phys. 65 (1989) 3610 "Electroluminescence of doped organic thin films," *Journal of Applied Physics*, vol. 65, no. 9, p. 3610, May 1989, doi: doi:10.1063/1.343409

[23] I. Sokolik, R. Priestley, A. D. Walser, R. Dorsinville, and C. W. Tang, "Bimolecular reactions of singlet excitons in tris(8-hydroxyquinoline) aluminum," Appl. Phys. Lett., vol. 69, no. 27, pp. 4168–4170, Dec. 1996, doi: 10.1063/1.116974. https://doi.org/10.1063/1.116974

[24] A.D. Walser, R. Priestley, R. Dorsinville, "Temperature dependence of the singlet excited state lifetime in alq3," *Synthetic Metals*, vol. 102, no. 1, pp. 1552–1553, Jun. 1999, doi: 10.1016/S0379-6779(98)00558-X.

[25] S. Fujita, T. Nakazawa, M. Asano, and S. Fujita, "Comparative Study of Photoluminescence Dynamics of Tris(8-hydroxyquinoline) Aluminum-Based Organic Multilayer Structures with Different Types of Energy Lineups," Jpn. J. Appl. Phys., vol. 39, no. 9R, p. 5301, Sep. 2000, doi: 10.1143/JJAP.39.5301.

[26] S. Kundu, K. Fujihara, T. Okada, and M. Matsumura, "Excitation Migration from Photoexcited Tris(8-hydroxyquinolino)aluminium to Quinacridone in Codeposited Thin Films," *Jpn. J. Appl. Phys.*, 39, 9R, (2000) 5297 doi: 10.1143/JJAP.39.5297.

[27] T. Mori, K. Obata, K. Miyachi, T. Mizutani, and Y. Kawakami, "Fluorescence Lifetime of Organic Thin Films Alternately Deposited with Diamine Derivative and Aluminum Quinoline," Jpn. J. Appl. Phys., vol. 36, no. 12R, p. 7239, Dec. 1997, doi: 10.1143/JJAP.36.7239.

[28] S. Zhang, J. Song, T. Kreouzis, and W. P. Gillin, "Measurement of the intersystem crossing rate in aluminum tris(8-hydroxyquinoline) and its modulation by an applied magnetic field," Journal of Applied Physics, vol. 106, no. 4, p. 043511, Aug. 2009, doi: 10.1063/1.3204015.

[29] J. Kido, H. Hayase, K. Hongawa, K. Nagai and K. Okuyama (1994), 'Bright red light-emitting organic electroluminescent devices having a europium complex as an emitter', Applied Physics Letters, 65, 2124 – 2126, DOI 10.1063/1.112810

[30] Yifan Zhang, Excited State Interactions and Management in Organic Light Emitting Diodes, thesis University of Michigan 2014.

[31] A. C. Chime, A. P. A. Fischer, S. Bensmida, J. Solard, M. Chakaroun, and H. Nkwawo, "Analysis of Optical and Electrical Responses of μ-OLED With Metallized ITO Coplanar Waveguide Electrodes Submitted to Nanosecond Electrical Pulses," IEEE Transactions on Electron Devices, vol. 66, no. 5, pp. 2282–2289, May 2019, doi: 10.1109/TED.2019.2905839.

[32] I. D. W. Samuel, and G. A. Turnbull, "Organic Semiconductor Lasers," Chem. Rev. vol. 107, no. 4, pp. 1272–1295, Apr. 2007. DOI: 10.1021/cr050152i13

[33] A.Uddin and C.B. Lee, "Exciton behaviours in doped tris(8-hydroxyquinoline) aluminium (Alq3) films", Phys. Status Solidi C 8, No. 1, 80–83, (2011), DOI.10.1002/pssc.201000429

[34] M. Lehnhardt, T. Riedl, T. Rabe, and W. Kowalsky, "Room temperature lifetime of triplet excitons in fuorescent host/guest systems", Organic Electronics 12, 486-491, (2011). DOI 10.1016/j.orgel.2010.12.017

[35] C.-W. Chang, Y.-T. Kao, and E. W.-G. Diau, "Fluorescence lifetime and nonradiative relaxation dynamics of DCM in nonpolar solvent," Chemical Physics Letters, vol. 374, no. 1–2, pp. 110–118, Jun. 2003, doi: 10.1016/S0009-2614(03)00645-6.

[36] J. Ohtsubo, Semiconductor Lasers: Stability, Instability and Chaos, 3rd ed. Berlin Heidelberg: Springer-Verlag, 2013.

[37] Lei Zeng *et al.*, "Electrical and Optical Impulse Response of High-Speed Micro-OLEDs Under UltraShort Pulse Excitation,"

IEEE Transactions on Electron Devices, vol. 64, no. 7, pp. 2942–2948, Jul. 2017, doi: 10.1109/TED.2017.2706723.

[38] A. C. Chime, S. Bensmida, M. Chakaroun, M. W. Lee, H. Nkwawo, and A. P. A. Fischer, "Electrical modelling and design of ultra-fast micro-OLED with coplanar wave-guided electrodes in ON-OFF regime," Organic Electronics, vol. 56, pp. 284–290, May 2018, DOI: 10.1016/j.orgel.2017.12.026

[39] We thank the reviewer for pointing this out.